Journal of Solid State Chemistry 184 (2011) 2238–2243

Contents lists available at ScienceDirect

Journal of Solid State Chemistry

journal homepage: www.elsevier.com/locate/jssc

X-ray photoelectron (XPS) and Diffuse Reflectance Infra Fourier Transformation (DRIFT) study of $Ba_{0.5}Sr_{0.5}Co_xFe_{1-x}O_{3-\delta}$ (BSCF: $x=0$–0.8) ceramics

Jae-Il Jung*, Doreen D. Edwards

Kazuo Inamori School of Engineering, Alfred University, Alfred, NY 14802, USA

ARTICLE INFO

Article history:
Received 31 January 2011
Received in revised form
8 June 2011
Accepted 20 June 2011
Available online 25 June 2011

Keywords:
BSCF
Barium strontium cobalt iron oxide
Perovskite
X-ray photoelectron
Diffuse Reflectance Infra Fourier Transformation
Binding energy

ABSTRACT

The X-ray photoelectron spectra (XPS) of sintered BSCF ceramics ($Ba_{0.5}Sr_{0.5}Co_xFe_{1-x}O_{3-\delta}$, $0 \le x \le 0.8$) were measured at room temperature (RT). Peak areas of Fe_{2p1}, Fe_{2p3}, Fe_{3p} and Co_{3p} increased systematically with increasing cobalt concentration, while their binding energies (BEs) remained the same (723.3, 710.0, 55.0 and 60.9 eV, respectively). However, the BEs of lattice oxygen in O_{1s} (528.1 eV) and Ba_{4d} for the BaO bond (87.9V and 90.2 eV) increased with increasing cobalt concentration. The shoulder peak of Ba_{3d}/Co_{2p} increased from 778.0 to 778.7 eV, which implies that this peak can be attributed to another Ba XPS peak (described as Ba_{2nd} in this study) due to the overlapping area between barium cations and oxygen anions. The overall peak areas of Ba_{4d} increased up to $x=0.4$, and then decreased, which coincides with the behavior of the Diffuse Reflectance Infrared Fourier Transform (DRIFT) bands representing adsorbed CO_3^{2-} (νCO_3^{2-}) and structurally bonded CO_3^{2-} (ν_2, ν_3) (800–1200 and 862/1433 cm^{-1}, respectively).

1. Introduction

The perovskite $Ba_{0.5}Sr_{0.5}Co_{0.8}Fe_{0.2}O_{3-\delta}$ (BSCF5582) has attracted considerable attention for its potential application as a cathode material in the intermediate temperature solid oxide fuel cells (IT-SOFCs) and oxygen separation membranes [1,2]. BSCF as a mixed ionic-electronic conductor (MIEC) exhibits a high oxygen-ionic transport rate via oxygen vacancies, with the oxygen self-diffusion coefficient and ionic conductivity on the order of 10^{-6} cm^2/s and 0.018 S/cm at 700 °C [3]. Such outstanding conducting properties as well as relatively high phase stabilities make it possible for BSCFs to be applied as semipermeable membranes and catalytic converter of hydrocarbons [4]. The substantial analyses of the surfaces of BSCF in diverse aspects such as crystalline structure and ionic binding energy can be helpful in designing BSCFs for the future applications.

BSCF possesses a cubic perovskite structure. B-site metal ions (Co, Fe) are coordinated by six oxygen ions to form close packing of BO_6 octahedral sites. A-site ions (Ba^{2+}(1.61 Å), Sr^{2+}(1.44 Å)) are coordinated by 12 adjacent oxygen ions and fitted between the BO_6 octahedra. The ideal lattice parameter, a, can be obtained with $a=\sqrt{2}(R_A+R_O)$ or $2(R_B+R_O)$ on the ground that R_A (Ba^{2+})=1.61 Å, R_B (Fe^{4+})=0.59 Å and R_O (O^{2-})=1.40 Å. If the lattice parameter, a, is equal to $\sqrt{2}(R_A+R_O)$, the calculated lattice parameter can be about 4.25 Å. On the other hand, the calculated lattice parameter with $a=2$ (R_B+R_O) will be about 3.97 Å.

The BO_6 octahedral determines lattice constant with $a=2(R_B+R_O)$, implied by the measured lattice constant by XRD analysis (around 3.95 Å) [5]. Therefore, it is expected that the electron clouds surrounding A-site cations could be overlapped with those of oxygen anions because of the shortened distance between A-site cations (especially Ba^{2+}) and oxygen anions in BSCF. Particularly, the bonding states between Ba cations and oxygen anions influence the BE of e^- using XPS spectra [6]. Also, the non-ideal crystal structure keeps a significant concentration of oxygen vacancies, which would also affect the unit cell volume size. In addition to the unit cell volume expansion, the calculated tolerance factor (t_f) increases from 1.042 to 1.052 as cobalt concentration increases from $x=0$ to 0.8 in $Ba_{0.5}Sr_{0.5}Co_xFe_{1-x}O_{3-\delta}$ according to [7]

$$t_f = \frac{(0.5*r_{Ba^{2+}} + 0.5*r_{Sr^{2+}} + r_{O^{2-}})}{\sqrt{2}(x*0.4*r_{Co^{3+}} + x*0.6*r_{Co^{4+}} + (1-x)*r_{Fe^{4+}} + r_{O^{2-}})} \quad (1)$$

where $r_{Ba2+}=1.61$ Å, $r_{Sr2+}=1.44$ Å, $r_{Co4+}=0.53$ Å, $r_{Co3+}=0.61$ Å, $r_{Fe4+}=0.59$ Å, $r_{Fe3+}=0.65$ Å and $r_{O2-}=1.40$ Å [8]. The comparison between the increases of lattice parameter and tolerance factor according to cobalt concentration increase is summarized in Table 1. Reaney et al. reported that the dielectric permittivity of

* Corresponding author: Fax: +1 864 656 5973.
E-mail address: jungji6013@hotmail.com (J.-I. Jung).

0022-4596/$ - see front matter © 2011 Elsevier Inc. All rights reserved.
doi:10.1016/j.jssc.2011.06.016

Ba- and Sr-based perovskite deviates significantly from the temperature referenced values when tolerance factor (t_f) are between 0.95 and 1.06 [9]. When t_f deviates from this range, the crystal structure is prone to be unstable. Therefore, the change of bonding state due to unit cell expansion and the increase of t_f with increasing cobalt concentration can affect the binding energy (BE) of e^- to each atom of BSCF.

The XPS BE (eV) shift is the chemical shift which changes according to differences in formal oxidation state, molecular environment, lattice site and so forth. The chemical shift effect can be explained with the charge potential model as shown in

$$E_i = E_i^o + kq_i + \sum_{i \neq j} \frac{q_i}{r_{ij}} \quad (2)$$

where E_i is the BE of a particular core level on atom i, E_i^o is an energy reference, q_i is the charge on atom i and the final term sums the potential atom at atom i due to 'point changes' on surrounding atoms j, which is also referred to as a Madelung potential [10]. The change in the valence electron density of Δq_i changes the potential inside the sphere by $\Delta q_i/r_v$, and the BE as well, where q_i has the opposite charge to atom. For an example, the decrease in valence electron density on atom i will cause the increase of BE, which can be achieved by the increase of bond length between atoms. Vasquez et al. reported that, as the XPS BE of $Ba_{4d5/2}$ increases from 87.2 to 88.0 eV, the Ba–O bond length linearly increases from 2.802 to 2.818 Å in Tl–cuprate system, which is expected from the Madelung energy change [6]. Borca et al. reported that the main two O_{1s} peaks observed in $La_{0.7}Ca_{0.3}MnO_3$ can be assigned to the perovskite structure (i.e., the peak at lower binding energy (528.7–529.0 eV) to the O_{1s} of the Mn–O layer, and the peak at 531.0 eV to O_{1s} of the La/Ca−O)

Table 1
Tolerance factor (t_f) and lattice parameter (a) as x increases in $Ba_{0.5}Sr_{0.5}Co_xFe_{1-x}O_{3-\delta}$.

	Tolerance factor (t_f)	Lattice parameter (a), Å
0	1.042	3.931
0.2	1.044	3.951
0.4	1.047	3.968
0.6	1.049	3.978
0.8	1.052	3.986

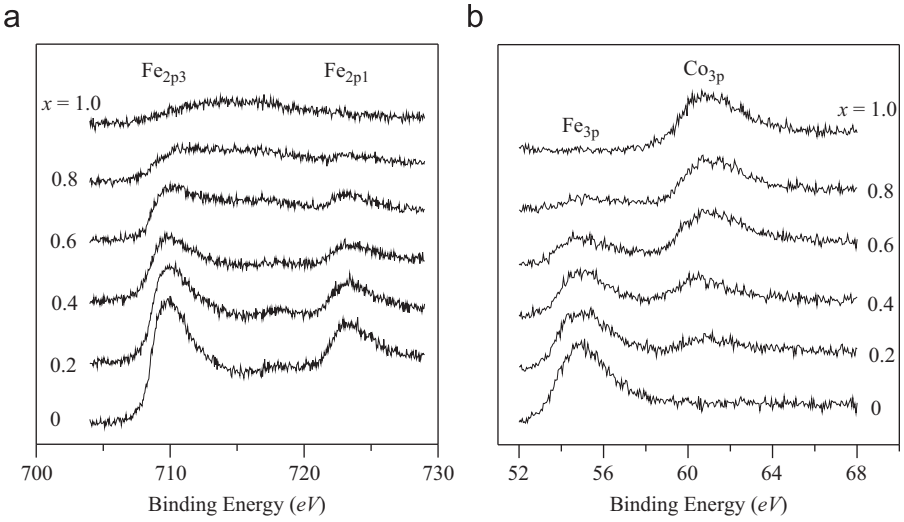

Fig. 1. The XPS spectra of (a) Fe_{2p} and (b) Co_{3p}/Fe_{3p} for the fractured surfaces of sintered $Ba_{0.5}Sr_{0.5}Co_xFe_{1-x}O_{3-\delta}$ samples.

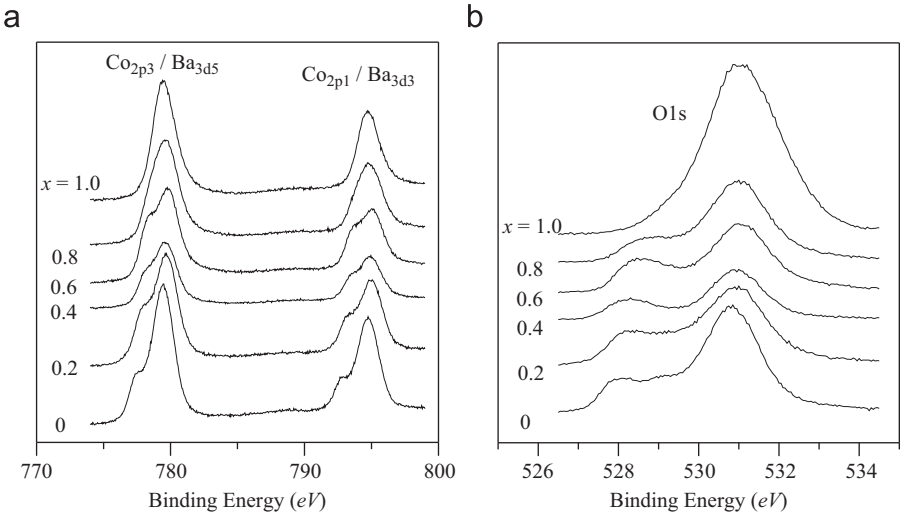

Fig. 2. The XPS spectra of (a) Co_{2p}/Ba_{3d} and (b) O_{1s} for the fractured surfaces of sintered $Ba_{0.5}Sr_{0.5}Co_xFe_{1-x}O_{3-\delta}$ samples.

[11–13]. Therefore, the quantitative comparison of XPS BE and peak area indicate substantial reaction or bonding between the cations (A-, B-site ions) and the anions (O^{2-}, O_2^-/O^-, CO_3^{2-}), which will eventually contribute to better understanding the surface state of BSCF.

This paper focuses on the analysis of XPS BE and peak area for each cation and oxygen anion in $Ba_{0.5}Sr_{0.5}Co_xFe_{1-x}O_{3-\delta}$ ($0 \le x \le 1$). The samples were prepared as fractured surfaces of sintered pellets and analyzed within a vacuum chamber. The high temperature DRIFT (Diffuse Reflectance Infrared Fourier Transform) spectra for $Ba_{0.5}Sr_{0.5}Co_xFe_{1-x}O_{3-\delta}$ ($0 \le x \le 1$) were analyzed on calcined powders under a constant flow of 30 ml dry air ($\le$ 10 ppm of moisture) within the closed chamber.

2. Experimental

$Ba_{0.5}Sr_{0.5}Co_xFe_{1-x}O_{3-\delta}$ powders were prepared using a polymerized complex method reported previously in the literature [5]. The starting materials consist of barium nitrate ($Ba(NO_3)_2$, $\ge$99.0% purity, Alfar Aesar Co.), strontium nitrate ($Sr(NO_3)_2$, $\ge$99.0% purity, Aldrich Chemical Co.), cobalt(II) nitrate ($Co(NO_3)_2 \cdot 6H_2O$, $\ge$99.0% purity, Alfar Aesar Co.), and iron(III) nitrate ($Fe(NO_3)_3 \cdot 9H_2O$, $\ge$98.0% purity, Alfar Aesar Co.). A 0.04 mol quantity of ethylenediamine tetraacetic acid (EDTA) was mixed with 40 ml of 1 N NH_4OH solution to make a NH_4–EDTA buffer solution. Equal molar amounts of barium nitrate (0.01 mol) and strontium nitrate (0.01 mol) and x (0, 0.004, 0.008, 0.012, or 0.016)mol of $Co(NO_3)_2 \cdot 6H_2O$ and (0.02–x) mol of $Fe(NO_3)_3 \cdot 9H_2O$, were added to the buffer solution to make the required stoichiometries of $Ba_{0.5}Sr_{0.5}Co_xFe_{1-x}O_{3-\delta}$ (x=0.0, 0.2, 0.4, 0.6, 0.8). Anhydrous citric acid (0.06 mol) was added, and the pH value was adjusted to 8 by using 1 N NH_4OH solution. Each solution was kept on a hot plate at 100 °C and stirred until gelation occurred. After 24 h, the gelled samples were baked in a drying oven at 200 °C for 6 h. The as-produced powders were then calcined at 950 °C for 7 h in air. The synthesized powders were pressed into pellets at 150 MPa. The samples were sintered at 1100 °C for 4 h in the air at a heating rate of 4 °C/min.

Table 2
Deconvoluted results of Co_{2p}/Ba_{3d} for $Ba_{0.5}Sr_{0.5}Co_xFe_{1-x}O_{3-\delta}$ XPS spectra.

x	BE		Area		Normalized area	
	~778 eV	780.1 eV	~778 eV	780.1 eV	~778 eV	780.1 eV
0.0	777.4	779.4	2900	15055	0.16	0.84
0.2	777.8	779.7	3642	12384	0.23	0.77
0.4	778.4	780.2	1404	7696	0.15	0.85
0.6	778.1	779.7	2577	10939	0.19	0.81
0.8	778.3	779.6	693	13579	0.05	0.95
1.0	779.2	779.7	3216	10977	0.23	0.77

For XPS analysis, the sintered bulk pellets were cleaved into neatly fractured surfaces by putting samples between sharp blades fastened to a contrived jig and hammering slightly on the top plate of the jig. The fastened blades fixed to plates are mobile just vertically enough to cut through intended spots of samples without moving horizontally. The fractured samples are inserted into XPS vacuum chamber within 5 min in order to minimize atmosphere contamination. Samples were kept within vacuum chamber for 30 h before measurements in order to pursue the ideal experimental conditions. Before measurement, there was neither Ar nor ion cleansing process on the fracture surface, because there could be the risk of washing selective atoms away during cleansing.

The XPS measurements were performed on a PHI Quantera SXM^{TM} instrument (ULVAC-PHI. Inc., JAPAN) (base pressure 5×10^{-9} Pa) using monochromatic Al $K\alpha$ radiation (1486.6 eV). The analyzer pass energy was set to 26 eV for narrow scans, the step size of which was 0.05 eV. The number of sweeps was 2 and the signal ratio to noise was 50. The energy scale was calibrated using the Ag_{4d} peak positions. The spot size of beam on sample was ~100 μm. The shifts in energy (charging) of the XPS spectra were corrected using the C_{1s} peak at 284.6 eV as a reference peak.

DRIFT (Diffuse Reflectance Infrared Fourier Transform) spectra were measured for powder samples within the closed chamber of a Nexus 670 FT-IR E.S.D.^{TM} (GMI Inc., USA) under the constant flow of 30 ml dry air ($\le$10 ppm of moisture) from room temperature (RT) to 700 °C, by heating the sample in 100°C increments, and holding at each step for 20 min.

3. Result

Fig. 1(a) shows the XPS data of Fe_{2p} level for the fractured surface of cleaved samples. The peak intensities and areas systematically decrease with increasing cobalt concentration in BSCF (x in $Ba_{0.5}Sr_{0.5}Co_xFe_{1-x}O_{3-\delta}$). The peaks of $Fe_{2p3/2}$ level become broader and more asymmetric toward the high BE as x increases. The BE locations of the $Fe_{2p3/2}$ peaks does not change according to x change. The peak BEs of 710.0 and 723.3 eV are assigned to $Fe_{2p3/2}$ and $Fe_{2p1/2}$, respectively, which represent Fe^{3+} species. The satellite peak occurring at approximately 8.0 eV above the $Fe_{2p3/2}$ is also characteristic of Fe^{3+} species [14]. It is difficult to distinguish between Fe^{3+} and Fe^{4+} [15]. Mori et al. reported that Fe^{3+} coexists with Fe^{4+} at RT with oxygen deficiency in $BaFeO_{3-\delta}$ [16]. Falcon et al. reported that the bonding strength of Fe^{3+}–O^{2-} and Fe^{4+}–O^{2-} are almost identical [17].

We therefore conclude that the valence of Fe stays as a mixture of +4 and +3 oxidation states, although Fe ions (primarily as +4) are in higher valence than Co ions (primarily as +3) in $Ba_{0.5}Sr_{0.5}Co_xFe_{1-x}O_{3-\delta}$ [5,14]. Fig. 1(b) shows the main peaks of Fe_{3p} and Co_{3p} spectra at 55.0 and 60.9 eV, respectively. All of the peaks are quite symmetric within the deviation of

Table 3
Deconvoluted results of O_{1s} for $Ba_{0.5}Sr_{0.5}Co_xFe_{1-x}O_{3-\delta}$ XPS spectra.

x	BE			Area			Normalized area		
	~528 eV	529.4 eV	531 eV	~528 eV	529.4 eV	531 Ev	~528 eV	529.4 eV	531 eV
0.0	528	529	530.8	904	1175	7195	0.10	0.13	0.78
0.2	528.1	529	530.9	722	1382	5460	0.10	0.18	0.72
0.4	528.1	528.7	530.9	330	446	3133	0.08	0.11	0.80
0.6	528.3	529.1	531	913	820	4952	0.14	0.12	0.74
0.8	528.5	529.2	531	633	548	5987	0.14	0.08	0.84
1.0	–	529.1	531.1	–	535	14443	–	0.04	0.96

± 0.2 eV and increase systematically in their areas and intensities according to increasing x in BSCF.

The main peaks at 780.1 eV in Fig. 2(a) are assigned to both $Co_{2p3/2}$ and $Ba_{3d5/2}$ simultaneously in the perovskite structure of BSCF [18], the locations of which peaks stay within the range of ± 0.24 eV deviation as the cobalt concentration increases. The peaks of which are indistinguishable from each other. The peak around 780.0 eV in the $Co_{2p3/2}$ typically represents Co^{3+}. An additional peak of the Co^{4+} state, generally located at higher BE, is not observed in this study [6]. On the other hand, at ~778.0 eV, there are satellite peaks which Falcon et al. suggest to be due to oxygen deficiency within perovskite structure [17]. Fig. 2(a) shows that, as x increases, the locations of satellite peaks shift to higher BE and are eventually absorbed into one large peak of $x=1.0$, as summarized in Table 2. The normalized areas were calculated as a ratio for each corresponding peak area.

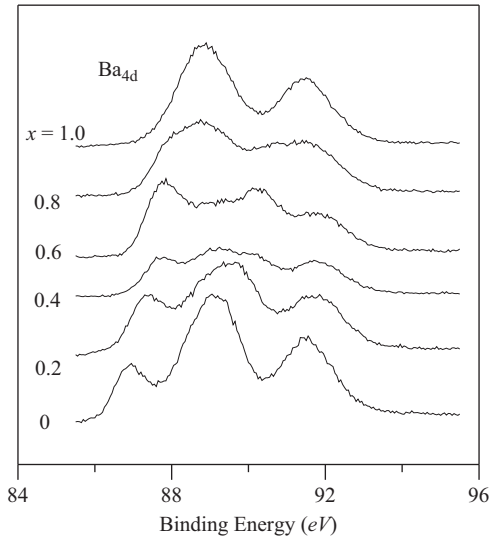

Fig. 3. The XPS spectra of the Ba_{4d} for the fractured surfaces of sintered $Ba_{0.5}Sr_{0.5}Co_xFe_{1-x}O_{3-\delta}$ samples.

Fig. 2(b) shows the O_{1s} spectra for BSCF. The O_{1s} spectrum at BSF($x=0$) presents three peaks, with BE values at 528.1, 529.2 and 531.0 eV. The lowest binding energy peak may be ascribed to the lattice oxygen species, O^{2-}, which systematically decreases in area with increasing cobalt concentration, as shown in Table 3. The peak location also shifts to higher BE as x increases, similar to the behavior of Co_{2p}/Ba_{3d} of Fig. 2(a). The middle peak (529.2 eV) is assigned to less adsorbed oxygen species, O_2^{2-}/O^-, referred to as electrophilic oxygen and known to actively degrade the carbon skeleton [19]. The decomposed carbonate (CO_3^{2-}) is expected to adsorb on the surface of BSCF ceramics. The noticeable peak area at 529.4 eV of $x=0$ (BSF) decreases from 1175 (0.13 as normalized area) to 446 (0.11) up to $x=0.4$ and mixes with the peaks of O^{2-} above $x=0.4$. The area of the highest BE peak (531.0 eV) which corresponds to CO_3^{2-} or OH^- (CO_3^{2-}/OH^-) [19,20] decreases up to $x=0.4$, and then increases above $x=0.4$. It is noticeable that, as x increases up to $x=0.4$, the peak area changes to the middle and highest BE peaks are nearly simultaneous, as summarized in Table 3.

Fig. 3 shows the spectra change in the Ba_{4d} according to the increase of x in BSCF. Each composition has multiple peaks. Miot et al. suggested that the peaks at 87.8 and 90.3 eV represent Ba_{4d} of BaO in the perovskite structure, while the peaks at 89.2V and 92.4 eV are assigned to Ba_{4d} of $BaCO_3$ [21,22]. The $BaCO_3$ is expected to come from the bonding between Ba cation and

Table 4
Deconvoluted results of Ba_{4d} for $Ba_{0.5}Sr_{0.5}Co_xFe_{1-x}O_{3-\delta}$ XPS spectra.

x	Peak shift				Area				Normalized area			
	87.9 eV	89.2 eV	90.2 eV	92.4 eV	87.9	89.2	90.2	92.4	87.9	89.2	90.2	92.4
0.0	86.9	88.22	89.2	91.48	778	921	2890	2035	0.12	0.14	0.44	0.31
0.2	87.39	88.77	89.75	91.71	1060	1294	1626	1580	0.19	0.23	0.29	0.28
0.4	87.71	89.11	90.23	91.76	593	1173	516	851	0.19	0.37	0.16	0.27
0.6	87.74	88.84	90.2	91.77	1024	1206	1323	1010	0.22	0.26	0.29	0.22
0.8	88.12	89.06	90.5	91.72	1076	1231	1134	1032	0.24	0.28	0.25	0.23
1.0	88.65	89.06	89.62	91.48	1950	364	606	1887	0.41	0.08	0.13	0.39

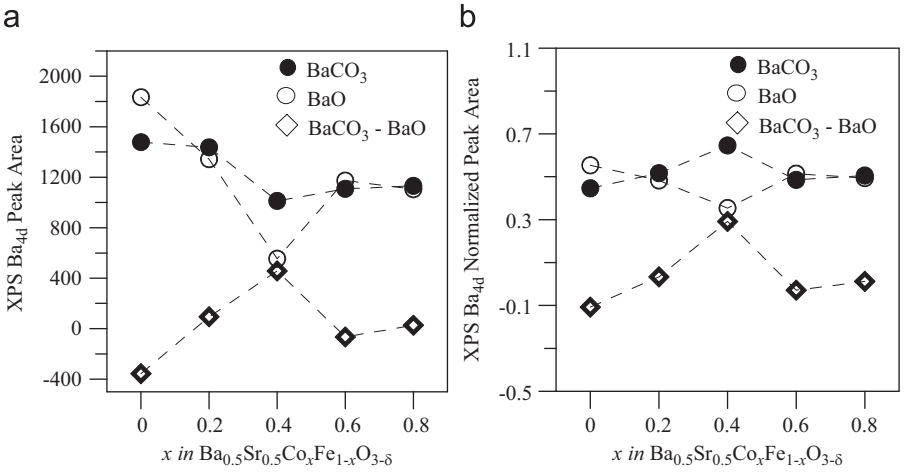

Fig. 4. The summary of (a) Ba_{4d} XPS spectra area and (b) normalized Ba_{4d} XPS spectra area of BaO and BaC for the fractured surfaces of sintered $Ba_{0.5}Sr_{0.5}Co_xFe_{1-x}O_{3-\delta}$ samples.

degraded carbonate (CO_3^{2-}) at the surface of BSCF, the reaction of which is promoted by the electrophilic oxygen species, O_2^{2-}/O^-, as explained in Fig. 2(b) and Table 3. Table 4 summarizes the peak shifts and areas for the corresponding Ba_{4d} peaks, after the spectra of each composition in Fig. 3 are deconvoluted. With increasing x, the overall peak locations shift to the higher BE, which coincides with the trend for Co_{2p}/Ba_{3p} and O_{1s}, and implies the systematic unit cell expansion [6]. This means that the structural expansion, which is mainly determined by R_B+R_O, does affect the bonding state between Ba^{2+} cations and oxygen anions such as O^{2-}, O_2^-/O^-, CO_3^{2-}/OH^-, while the BEs of Fe_{2p}, Fe_{3p} and Co_{3p} do not change. On the other hand, the overall peak areas of Ba_{4d} in Fig. 3 and Table 4 decrease up to $x=0.4$ and then increase above $x=0.4$, both for BaO (87.9 and 90.2 eV) and $BaCO_3$ (89.2 and 92.4 eV).

When the average values of peak area for BaO and $BaCO_3$ are plotted against x of $Ba_{0.5}Sr_{0.5}Co_xFe_{1-x}O_{3-\delta}$, the decreasing and increasing rate of peak area for BaO is greater than for $BaCO_3$ with a transitional point of $x=0.4$, as summarized in Fig. 4. When the peak areas for $BaCO_3$ are subtracted by those of BaO, the sum of overall peak areas (Δ = peak areas for $BaCO_3$ − peak areas for BaO) increases up to $x=0.4$, and then slightly diminishes after $x=0.4$, as shown in Fig. 4.

Fig. 5 shows the result of *in situ* DRIFT (Diffuse Reflectance Infrared Fourier Transform) spectra analysis for the whole compositional range of BSCF powder ($0 \le x \le 1$) as temperature increases from RT to 300 °C in air. The DRIFT bands at 862 and 1433 cm^{-1} (the wave numbers marked in Fig. 5) are assigned to the asymmetric stretching v_2 and v_3 modes, respectively, of CO_3^{2-} in $BaCO_3$ [23–26]. These bands increase up to $x=0.4$ and then diminish slightly above $x=0.4$, which is coincident with the trend of XPS peak area changes of Ba_{4d} for $BaCO_3$ bonds, as has been explained in Fig. 4. On the other hand, 800–1200 cm^{-1} region (marked in Fig. 5) represents adsorption bands related to νCO_3^{2-} [27,28]. These bands decrease up to $x=0.4$, and then show little change above $x=0.4$. This signifies that, as x increases in $Ba_{0.5}Sr_{0.5}Co_xFe_{1-x}O_{3-\delta}$, the number of $BaCO_3$ bonds increases at the consumption of adsorbed CO_3^{2-} up to $x=0.4$, and above $x=0.4$, DRIFT bands from both structurally bonded CO_3^{2-} (v_2, v_3) and adsorbed CO_3^{2-} (νCO_3^{2-}) are significantly lessened. The bands at 758 cm^{-1} (marked in Fig. 5) are assigned to ring def. + ν(Co–O_l) [29,30]. As x increases, these bands systematically increase up to $x=0.8$, but differently for BSC ($x=1$).

4. Discussion

With increasing cobalt concentration, the XPS BEs correlated with Ba–O bonds increased systematically, which is in line with the increasing unit cell volume and oxygen vacancy concentration. It is also noticeable that, even though the lattice parameter is determined by the bonding between B-site cations and oxygen anions, the XPS BEs of typical Fe and Co peaks does not shift. This signifies that increased lattice parameter accompanied by oxygen vacancy formation could significantly affect the BE of Ba and O. The high t_f of BSCF at the high cobalt concentration in BSCF implies that the electron densities of Ba and O can be overlapped.

As the lattice parameter increases, the electron density around Ba and O will decrease and Madelung potential will increase, which leads to the increase of BE, as shown in the Ba and O XPS peaks. This is observed by the increase of shoulder peaks in Co_{2p}/Ba_{3d}, ~778 eV from 777.4 to 778.3 eV.

Also, the subtracted peak area of $BaCO_3$ by BaO increased up to $x=0.4$ and then decreased, which matches with the increase of $BaCO_3$ (862 and 1433 cm^{-1}) in the DRIFT analysis. This can be attributed to the increase of v_2 and v_3 modes of CO_3^{2-} in $BaCO_3$ up to $x=0.4$ at the consumption of absorbed CO_3^{2-} (νCO_3^{2-}) which is expected to come from degraded carbon skeleton. This argument is supported by the decrease of νCO_3^{2-} bands (800–1200 cm^{-1}) up to $x=0.4$ in the DRIFT spectra.

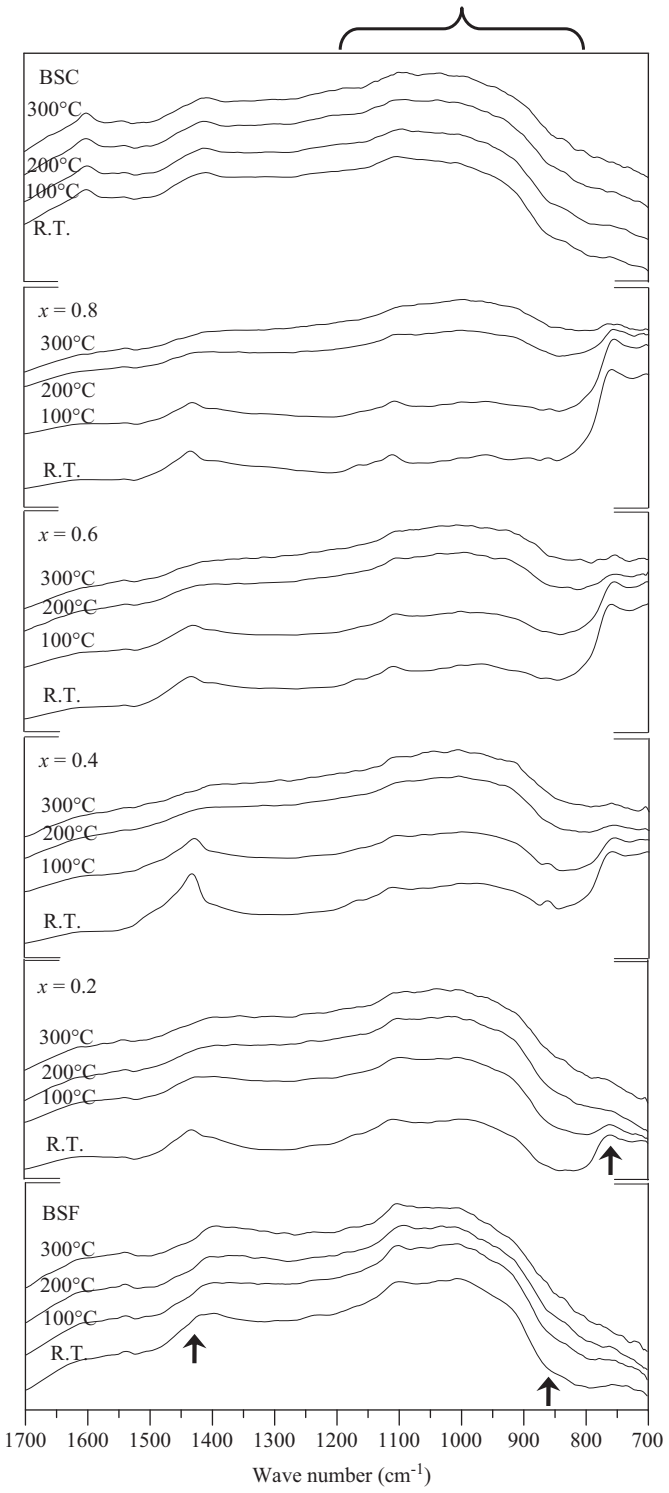

Fig. 5. DRIFT (Diffuse Reflectance Infra Fourier Transformation) spectra of calcined power of $Ba_{0.5}Sr_{0.5}Co_xFe_{1-x}O_{3-\delta}$ samples.

5. Conclusions

With increasing cobalt concentration, the XPS BEs of Ba_{4d} and O_{1s} increased, while the BEs representing Co and Fe did not

change, which can be explained by various arguments concerning lattice parameter, tolerance factor and the overlapped zone between Ba and O. For a more detailed explanation, a deeper study is required.

The systematic increase of Ba_{3d}/Co_{2p} shoulder XPS peak from 778.0 to 778.7 eV indicates that this peak belongs to another Ba_{3d} XPS peak coming from the overlapped area between barium cation and oxygen anion.

The relative increase in $BaCO_3$ peak areas over BaO explains that adsorbed CO_3^{2-} gets bonded to the crystalline into $BaCO_3$, which is supported by the decrease of those νCO_3^{2-} DRIFT bands (800–1200 cm^{-1}) up to $x=0.4$.

Acknowledgment

The author kindly acknowledges the insightful discussions of Dr. Robert A Condrate.

References

[1] Z. Shao, S.M. Halle, Nature 431 (2004) 170. doi:10.1038/nature02863.
[2] Z. Shao, W. Yang, Y. Kong, H. Dong, J. Tong, G. Xiong, J. Membr. Sci. 172 (2000) 177.
[3] E. Bucher, A. Egger, P. Ried, W. Sitte, P. Holtappels, Solid State Ionics 179 (2008) 1032.
[4] K. Efimov, Q. Xu, A. Feldhoff, Chem. Mater. 22 (2010) 5866.
[5] J. Ovenstone, J.I. Jung, J.S. White, D.D. Edwards, S.T. Misture, J. Solid State Chem. 181 (2008) 576.
[6] R.P. Vasquez, M.P. Siegal, D.L. Overmyer, Z.F. Ren, J.Y. Lao, J.H. Wang, Phys. Rev. B 60 (6) (1999) 4309.
[7] B.W. Liu, Y. Zhang, L. Tang, Int. J. Hydrogen Energy 34 (2009) 435.
[8] R. Shannon, Acta Crystallogr., Sect. A: Cryst. Phys. Diffr. Theor. Gen. Crystallogr. 32 (5) (1976) 751.
[9] I.M. Reaney, E.L. Colla, N. Setter, Jpn. J. Appl. Phys. 33 (1994) 3984.
[10] D. Briggs, M.P. Seah, Practical Surface Analysis by Auger and X-ray Photoelectron Spectroscopy, John Wiley & Sons, 1983, p. 119.
[11] C.N. Borca, S. Canulescu, F. Loviat, T. Lippert, D. Grolimund, M. Dobeli, J. Wambach, A. Wokaun, Appl. Surf. Sci. 254 (2007) 1352.
[12] E. Beyreuther, S. Grafström, L.M. Eng, C. Thiele, K. Dörr, Phys. Rev. B 73 (2006) 155425.
[13] J.W. Choi, J. Zhang, S.H. Liou, P.A. Dowben, E.W. Plummer, Phys. Rev. B 59 (20) (1999) 13453.
[14] P. Mills, J.L. Sullivan, J. Phys. D 16 (1983) 723.
[15] Y.G. Cho, K.H. Choi, Y.R. Kim, J.S. Jung, S.H. Lee, Bull. Korean Chem. Soc. 30 (6) (2009) 1368.
[16] K. Mori, T. Kamiyamaa, H. Kobayashi, K. Itoh, T. Otomo, S. Ikeda, Physica B 329–333 (2003) 807.
[17] H. Falcon, J.A. Barbero, J.A. Alonso, M.J. Martınez-Lope, J.L.G. Fierro, Chem. Mater. 14 (2002) 2325.
[18] E.A. Fardin, A.S. Holland, K. Ghorbani, P. Reichart, Appl. Phys. Lett. 89 (2006) 022901.
[19] N.A. Merino, B.P. Barbero, P. Eloy, L.E. Cadus, Appl. Surf. Sci. 253 (2006) 1489.
[20] S. Rousseau, S. Loridant, P. Delichere, A. Boreave, J.P. Deloume, P. Vernoux, Appl. Catal. B 88 (2009) 438.
[21] C. Miot, E. Husson, C. Proust, R. Erre, J.P. Coutures, J. Mater. Res. 12 (9) (1997) 2388.
[22] M. Viviani, M.T. Buscaglia, P. Nanni, R. Parodi, G. Gemme, A. Dacca, J. Eur. Ceram. Soc. 19 (1999) 1047.
[23] Y. Yang, Y. Jiang, Y. Wang, Y. Sun, J. Mol. Catal. A: Chem. 270 (2007) 56.
[24] K. Nakamoto (Ed.), Infrared and Raman Spectra of Inorganic and Coordination Compounds Part A, 6th Ed,John Wiley & Sons. Inc., NJ, 2009, pp 33, 183.
[25] D.H. Lee, Ph. D. thesis, Alfred University, 1998, pp. 2–3, 7–9.
[26] G. Busca, V. Buscaglia, M. Leoni, P. Nannit, Chem. Mater. 6 (1994) 955.
[27] L. Fornia, C. Oliva, T. Barzettia, E. Selli, A.M. Ezerets, A.V. Vishniakov, Appl. Catal. B 13 (1997) 35.
[28] J.M.D. Tascon, L.G. Tejuca, J. Chem. Soc. Faraday Trans. I 77 (1981) 591.
[29] J. Fujita, A.E. Martell, K. Nakamoto, J. Chem. Phys. 36 (1962) 339.
[30] K. Nakamoto (Ed.), Infrared and Raman Spectra of Inorganic and Coordination Compounds Part B, 6th Ed,John Wiley & Sons. Inc., NJ, 2009, pp 91.